

14.4a INFRARED THERMAL IMAGERY OF CLOUD BASE IN TORNADIC SUPERCELLS

Robin L. Tanamachi*

Howard B. Bluestein

School of Meteorology, University of Oklahoma, Norman, Oklahoma

Stephen S. Moore

Intrinsic Energies Indications, Saline, Michigan

Robert P. Madding

Infrared Training Center, FLIR Systems, Inc., Billerica, Massachusetts

Curtis R. Alexander

School of Meteorology, University of Oklahoma, Norman, Oklahoma

1. INTRODUCTION

It has been suggested that the temperature field in and near a low-level mesocyclone, particularly that associated with the rear-flank downdraft (RFD), may play a role in tornadogenesis (Davies-Jones *et al.* 2001; Lemon and Doswell 1979). Previous studies have sought to test this hypothesis using mobile in situ instruments to measure thermodynamic variables in and around the parent mesocyclone (Markowski *et al.* 2002; Bluestein 1999). However, safety concerns make the deployment of thermodynamic measuring instruments in close proximity to a tornadic mesocyclone extremely difficult.

Infrared thermal imagery, or thermography, can be used to infer the temperatures of objects within the images from their emitted long wave infrared radiances. Infrared thermal imagery is familiar to the general public through its industrial, military, and law enforcement applications. This study marks the first known use (to the best knowledge of the authors) of ground-based infrared thermography for severe storms research.

In this study, an infrared camera was used in an attempt to distinguish different stages in the life cycle of a tornado based on the measured thermal characteristics of the visible tornado and surrounding cloud base. The equipment used consisted of a tripod-mounted, digital, FLIR Systems brand S60 ThermoCam digital radiometric imager capable of detecting infrared radiation with wavelengths between 8 and 12 μm at a resolution of 640 x 480 pixels. The 8 – 12 μm band is a water vapor “window,” wherein water vapor has

relatively low emissivity and absorptivity and therefore a relatively small effect on atmospheric transmissivity.

Since the infrared camera is not dependent on the visible portion of the electromagnetic spectrum, the infrared camera also functions well in low light situations, leading the authors to speculate about the possibility of using infrared thermal imagery for nocturnal tornado detection and “storm spotting.”

The camera is also equipped with a low-resolution (640 x 480 pixels) digital camera to take pictures of the visible subject within a few seconds of the infrared image capture. Side-by-side analysis of the visible and infrared images is therefore possible.

The infrared camera was deployed near numerous supercell storms in 2003 and 2004. What follows is a discussion of the atmospheric transmissivity issues related to this study, and three highlighted cases in which side-by-side visible and infrared thermal images will be examined.

2. TRANSMISSIVITY STUDY

In order to determine the effect of atmospheric attenuation on the infrared signal from cloud base, an atmospheric transmissivity study was conducted. The procedure for this study involved the capture of infrared thermal images of low-level, cumuliform, non-precipitating water clouds above the National Weather Service (NWS) office in Norman, Oklahoma simultaneously with standard NWS rawinsonde launches from that location. Cloud-base temperatures measured by the infrared camera were then compared with the lower atmospheric profile measured by the rawinsonde. The transmissivity study made use of the assumption that (1) the cloud base height was in fact the same as the lifting condensation level

* Corresponding author address: Robin L. Tanamachi; Univ. of Oklahoma, School of Meteorology; 100 E. Boyd, Rm. 1310; Norman, OK 73019; e-mail: rtanamachi@ou.edu.

(LCL) height recorded by the rawinsonde, and (2) the cloud base temperature was in fact the same as the LCL temperature recorded by the rawinsonde. The small amount of heating caused by latent heat release from condensation (Wallace and Hobbs 1977) was assumed to be negligible for the purposes of this study since the temperature change due to this heating was within the range of spectral noise of the infrared camera ($< 2\text{ }^{\circ}\text{C}$).

Using simple trigonometry, the approximate line-of-sight distance from the infrared camera to a selected cloud base was computed from the elevation angle of the camera and the height of the LCL as recorded by the rawinsonde observations. The computed line-of-sight distance was entered into proprietary ThermaCam software intended to correct the measured temperatures in the images for clear-air atmospheric attenuation, using a simplified version of the MODTRAN radiative transfer model (Berk 1989). This software produced corrected temperatures and estimates of the atmospheric transmissivity.

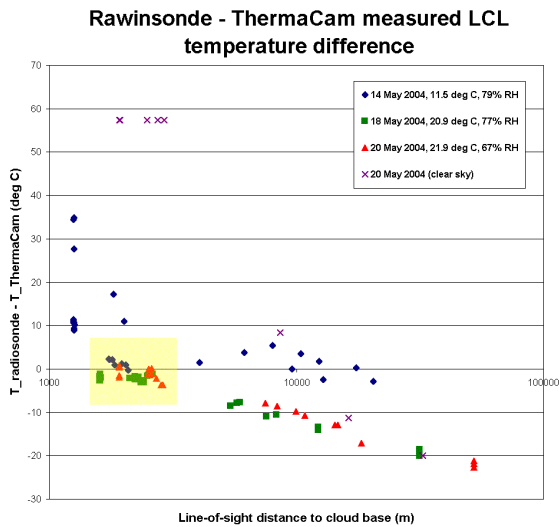


Figure 1. Difference in LCL temperature measured by an NWS rawinsonde and the infrared camera at 00 UTC on 15, 19, and 21 May 2004. Measurements of the clear sky were also taken on 20 May as a control. The yellow box encloses a region of optimum camera-to-cloud distance. The distance scale is logarithmic.

The difference between the temperature of the cloud base as measured by the infrared camera and the rawinsonde becomes more negative as the distance of the cloud base from the infrared camera increases. As the camera tilts towards the horizon, the optical depth of the intervening medium decreases owing to the relatively high concentrations of ozone and other infrared-emitting gases and particulates in the atmospheric boundary layer. In general, low clouds appear warmer than

their surroundings when the camera elevation angle is greater than 30° due to their contrast against cooler upper tropospheric air or colder clouds at higher elevations. As the camera elevation angle decreases to 0° and the field of view approaches the horizon, the infrared signal from the distant cloud base becomes obscured by the infrared signal from water vapor, ozone, and haze particles in the lower atmosphere. Therefore the temperature of the cloud base measured by the infrared camera will be too high.

The data from three such transmissivity studies are shown in Figure 1. The yellow box encloses a region that represents an optimum distance for temperature measurement between the camera and the cloud base, between approximately 1500 and 3000 m (1.5 and 3 km). In this region, the difference between the temperature measured by the rawinsonde and that measured by the infrared camera was most consistently close to zero; thus it is reasonable to suggest that 1.5 to 3 km is the best range from which to accurately study temperature changes across low cloud bases.

3. TORNADO DATA

During the spring seasons of 2003 and 2004, the infrared camera was deployed near supercell thunderstorms. The goal of each infrared camera deployment was the capture of infrared images within 3 km of a tornadic mesocyclone. The 3 km distance criterion, derived from the transmissivity study, was intended to ensure that the camera would be close enough to distinguish the infrared signal of the cloud base from that of the intervening atmosphere. The deployment occurred alongside a mobile radar unit whenever possible, in order to ascertain an accurate line-of-sight distance between the camera and any developing tornadoes.

3.1 11 June 2003: Kennebec, South Dakota

At approximately 2230 UTC on 11 June 2003, the infrared camera captured the images in Figure 2 from just north of the town of Kennebec, South Dakota. The visible image shows part of a horseshoe-shaped mesocyclone lowering underneath a low-precipitation supercell, the leading edge of which is located approximately 5 km west of the camera. A Doppler on Wheels (DOW) mobile radar documented a weak tornadic vortex within three minutes of this infrared image capture. No visible condensation funnel was observed.

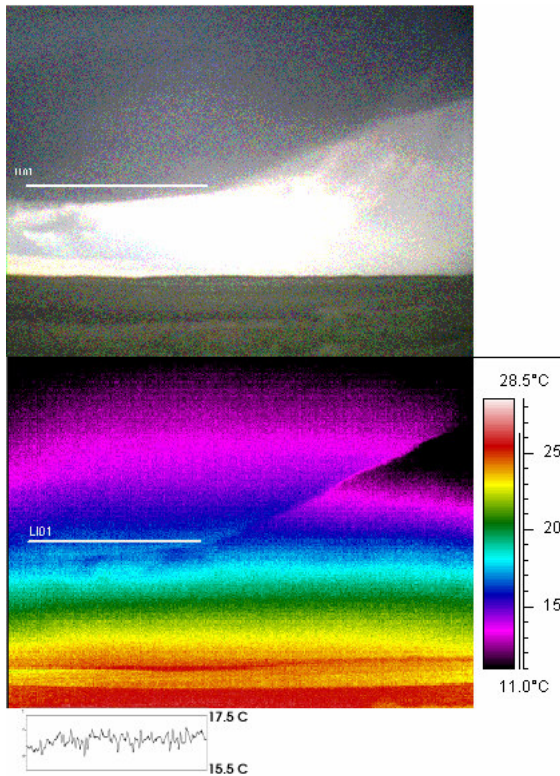


Figure 2. Visible (top) and infrared (middle) images of a cloud lowering underneath the Kennebec, South Dakota storm of 11 June 2004. These images were taken at 2230 UTC. The location of the radar-detected tornado is near the left edge of the image. The graph (bottom) is a trace of the temperature along the line (labeled LI01) in the infrared image.

In the infrared image, the mesocyclone lowering appears as an area of relatively warm temperatures contrasted against higher-altitude, cooler clouds above and behind. No temperature difference greater than that of instrument noise is observed across the base in the vicinity of the radar-indicated tornadic circulation.

3.2 12 May 2004: Harper Co., Kansas

Over 100 infrared images of tornadoes and their associated cloud base prior to tornadogenesis were captured on 12 May 2004 (local time) in Harper County, Kansas.

The team was fortunate enough to capture infrared images of the tornadogenesis phase. No temperature difference greater than that of instrument noise is observed across the mesocyclone lowering in the vicinity of the visible tornadic circulation (Figure 3).

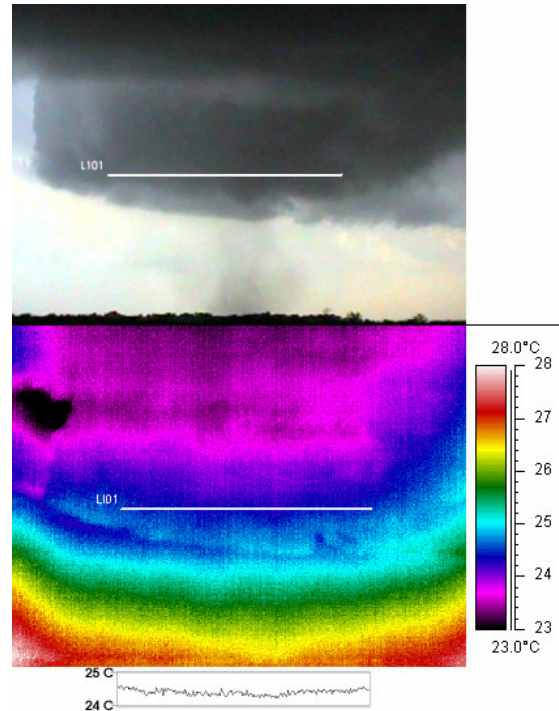


Figure 3. Visible (top) and infrared (middle) images of the tornadogenesis phase of a tornado that formed just east of Attica, KS on 13 May 2004, at around 0056 UTC. The graph (bottom) is a trace of the temperature along the line (labeled LI01) in the infrared image. The slight “bowing” of the isothermal color bands near the edges of the image is due to slight warming of the edges of the infrared detector array inside the camera. The detector array is automatically recalibrated every few seconds.

The tornado, in its mature phase, crossed U.S. Hwy 160 near Attica, KS at 0102 UTC on 13 May 2004. It appears in the infrared imagery (Figure 4) as a column of slightly elevated temperatures. This warming is probably due to the slight warming of the air in the funnel as water vapor condenses out of it. However, the infrared signal of the tornado condensation funnel was either very faint or nonexistent in many of the images, particularly near the ground, where, as the transmissivity study indicated, infrared signal contamination due to haze and lofted soil particles was probably high.

The further elevation of temperatures at the left and right edges of the condensation funnel is probably due to the ingestion of dust into the funnel from the warm surface soil layer. The dust particles are then centrifuged by the tornado to the outer edges of the tornado funnel (Dowell *et al.* 2001). At the edges of the condensation funnel, as can be seen in the visible image, this cylinder of dust is viewed from an oblique angle. There is more dust in the line-of-sight that passes from the infrared camera through the edge of the funnel;

thus the edges of the funnel appear warmer than the main body of the funnel itself, much as they appear darker than the funnel in the visible image.

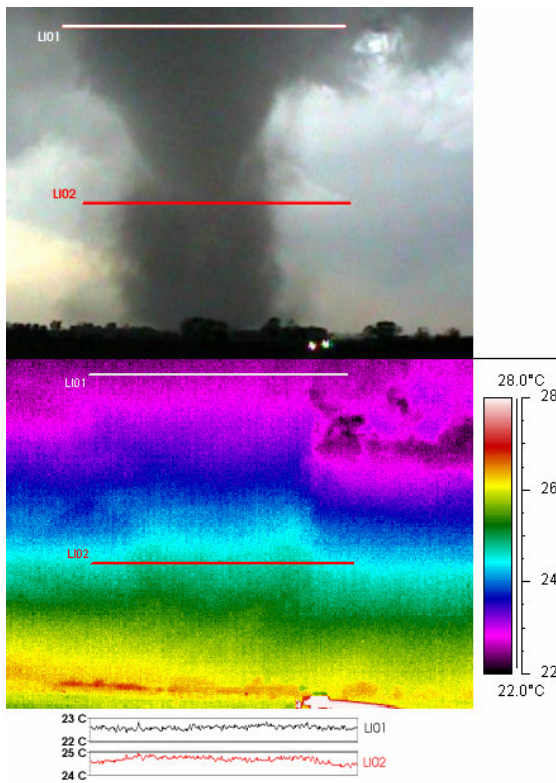


Figure 4. Visible (top) and infrared (middle) images of a tornado near Attica, KS at around 0102 UTC on 13 May 2004 (same tornado as in Figure 2). The tornado was located approximately 4.5 km from the camera at the time these images were taken. The graphs (bottom) are traces of the temperature along the lines (labeled LI01 and LI02) in the infrared image.

3.3 11 June 2004: Lehigh, Iowa

A sequence of 10 infrared images was captured on 11 June 2004, capturing both the mature and shrinking stages of a tornado near Lehigh, Iowa. Since the tornado was already in progress by the time the infrared camera could be deployed, no images were captured during tornadogenesis. Unfortunately, heavy rain curtains fell between the infrared camera and the tornado, and these rain curtains completely obscured the infrared signal of the condensation funnel as well as the temperatures of the air in the immediate vicinity of the tornado. An example is shown in Figure 5.

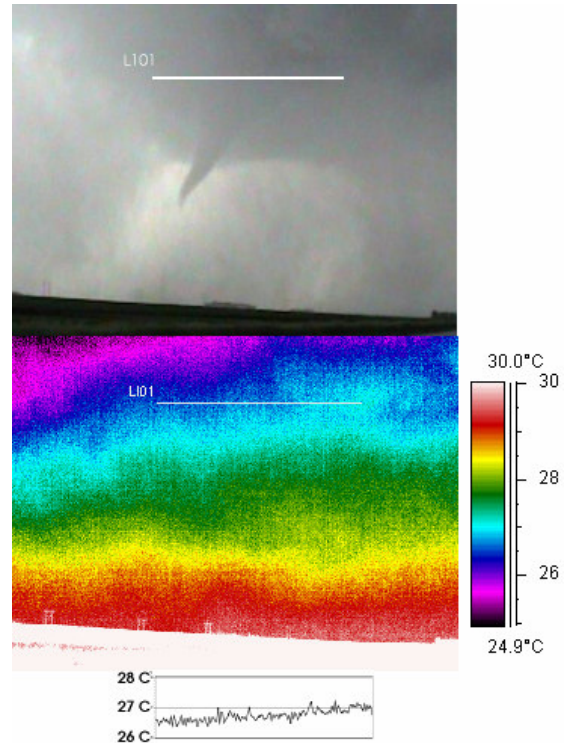


Figure 5. Visible (top) and infrared (middle) images of a tornado near Lehigh, Iowa at 0036 UTC on 12 June 2004 (11 June local time). The infrared signal of the condensation funnel (approximately 3.5 km away) is almost completely obscured by intervening rain curtains. The graph (bottom) is a trace of the temperature along the line (labeled LI01) in the infrared image. Heavy rain falling in the foreground on the left side of the image is the likely cause of the decrease in temperature near the upper-left corner of the image.

4. CONCLUSIONS

This study highlighted a number of difficulties inherent in infrared thermography in a severe thunderstorm situation: relatively high concentrations of haze and lofted soil particles in the warm sector decrease the infrared transmissivity of the atmosphere, requiring the thermographer to decrease his or her range to the subject.

Often the tornado is already in progress by the time the infrared camera can be deployed within 3 km; therefore the capture of images of tornadogenesis is extremely difficult.

Additionally, precipitation curtains between the infrared camera and the tornado can contaminate the infrared signal from the tornado funnel and cloud base. In the 11 June 2004 case, the precipitation curtains completely obscured the infrared signal of the tornado funnel.

As for the hypothesis that tornadogenesis may be related to the temperature gradients in the RFD, this study did not provide conclusive evidence supporting this hypothesis, largely because in each case the elevation angle of the infrared camera when pointed at the underside of the mesocyclone was too oblique to yield sufficiently detailed information about the mesocyclone structure. An “ideal” case would require that images be captured from within the 1.5 – 3 km range, clearly showing the presence of cold air from the RFD, and also include mesonet verification of the surface temperatures.

Given the relatively small range requirement of the infrared camera to the tornado, the thermographer must use his or her utmost discretion with regards to tornado safety. Lightning safety is also an issue, as the upright tripod and camera can both serve as lightning attractors in the event of a strike.

These factors, combined with the expense of the equipment, lead the authors to conclude that long wave infrared thermography is probably not a practical option for nocturnal storm spotting. However, studies using shortwave infrared thermography (colloquially known as “night vision”) have yet to be conducted.

5. ACKNOWLEDGMENTS

Thanks to Stephan P. Nelson of the National Science Foundation (NSF) for supporting this project under NSF SGER grant ATM-0332894. Gary Orlove of FLIR Systems, Inc. provided useful information about the transmissivity algorithm in the proprietary software. The authors are grateful to Dr. Joshua Wurman of the Center for Severe Weather Research in Boulder, Colorado for allowing the infrared camera to join the DOW storm intercept convoy for a portion of each of the 2003 and 2004 storm seasons, and for sharing DOW radar data for relevant cases.

6. REFERENCES

- Berk, A., L. S. Bernstein, and D. C. Robertson, 1989: MODTRAN: A moderate-resolution model for LOWTRAN 7. GL-TR-89-0122. 38 pp. [NTIS AD A214337.]
- Bluestein, H. B., 1999: A history of severe-storm-intercept field programs. *Wea. and Forec.*, 14, 558 – 577.
- Davies-Jones, R. P., R. J. Trapp, and H. B. Bluestein, 2001: Tornadoes and tornadic storms. *Severe Convective Storms*, Meteor.

Monogr., No. 28, Amer. Meteor. Soc., 167 – 221.

- Dowell, D. C., J. Wurman, and L. J. Wicker, 2001: Centrifuging of scatterers in tornadoes. Preprints, *30th Conf. on Radar Meteorology*, Munich, Germany, Amer. Meteor. Soc., 307–309.
- Lemon, L. R., and C. A. Doswell III, 1979: Severe thunderstorm evolution and mesocyclone structure as related to tornadogenesis. *Mon. Wea. Rev.*, **107**, 1184 – 1197.
- Liou, K. N., 2002: *An Introduction to Atmospheric Radiation*. 2nd ed. Academic Press, 583 pp.
- Markowski, P. M., J. M. Straka, and E. N. Rasmussen, 2002: Direct surface observations within the rear-flank downdrafts of non-tornadic and tornadic supercells. *Mon. Wea. Rev.*, **130**, 1692 – 1721.
- Wallace, J. M., and P. V. Hobbs, 1977: *Atmospheric Science: An Introductory Survey*. Academic Press, 467 pp.